Transport of Strontium and Cesium in Simulated Hanford Tank Waste Leachate through Quartz Sand under Saturated and Unsaturated Flow

ARTICLE *in* ENVIRONMENTAL SCIENCE & TECHNOLOGY · OCTOBER 2010

Impact Factor: 5.33 · DOI: 10.1021/es903223x · Source: PubMed

3 AUTHORS, INCLUDING:

Kenton A. Rod
Washington State University
11 PUBLICATIONS **61** CITATIONS
SEE PROFILE

Wooyong Um
Pacific Northwest National Laboratory
91 PUBLICATIONS **799** CITATIONS
SEE PROFILE

Transport of Strontium and Cesium in Simulated Hanford Tank Waste Leachate through Quartz Sand under Saturated and Unsaturated Flow

KENTON A. ROD,[†,‡] WOOYONG UM,[*,†] AND MARKUS FLURY[‡]

Pacific Northwest National Laboratory, P.O. Box 999, K3-62, 902 Battelle Boulevard, Richland, Washington 99354, Pacific Northwest National Laboratory, P.O. Box 999, P7-22, 902 Battelle Boulevard, Richland, Washington 99354, and Department of Crop and Soil Sciences, Washington State University, Pullman, Washington 99164-6420

Received February 18, 2009. Revised manuscript received September 1, 2010. Accepted September 14, 2010.

We investigated the effects of water saturation and secondary precipitate formation on Sr and Cs transport through quartz sand columns under saturated and unsaturated flow. Column experiments were conducted at effective water saturation ranging from 0.2 to 1.0 under steady-state flow using either 0.1 M $NaNO_3$ or simulated tank waste leachate (STWL; 1 M $NaNO_3$ and 1 M NaOH) mimicking Hanford (Washington, USA) tank waste. In 0.1 M $NaNO_3$ columns, Sr transported like a conservative tracer, whereas Cs was retarded relative to Sr. The transport of Sr and Cs in the 0.1 M $NaNO_3$ columns under all water saturations could be described with the equilibrium convection-dispersion equation (CDE). In STWL columns, Sr mobility was significantly reduced compared to the 0.1 M $NaNO_3$ column, because Sr was incorporated into or sorbed to neo-formed secondary precipitates. Strontium sequestration by precipitates was confirmed by additional batch and electron micrograph analyses. In contrast, the transport of Cs was less affected by the STWL; retardation of Cs in STWL columns was similar to that found in 0.1 M $NaNO_3$ columns. Analysis of STWL column data revealed that both Sr and Cs breakthrough curves showed nonideal behavior that suggest nonequilibrium conditions, although nonlinear geochemical behavior cannot be ruled out.

Introduction

High-level radioactive waste, generated as a result of Pu refinement at the US Department of Energy's Hanford Reservation, has been stored in large underground tanks. Sixty-seven out of the 177 single shell tanks have been found to be leaking (*1*). Although different chemical compositions were reported, in general, the Hanford tank waste is characterized as a caustic (pH = 9 to 14) and high-ionic strength (I = 2 to 14 M) solution with high concentration of dissolved Al (*2, 3*). In the waste solutions, contaminants of concern are ^{90}Sr and ^{137}Cs found at activities as high as 11.1 GBq L^{-1} (0.3 Ci L^{-1}) and 5.55 GBq L^{-1} (0.15 Ci L^{-1}), respectively (*3*). Flow of the leaking solution in the vadose zone is characterized by changes in flow paths and velocity due to varying soil moisture, the heterogeneous characteristics of the sediments, and mineral dissolution and precipitation after contact (*4*).

Geochemical changes occur when hyper-alkaline caustic solutions come into contact with quartz sand or sand-dominated Hanford sediments (*5*−*10*). The caustic leachate dissolves silicate minerals, and the dissolved Si can react with Al, Na, and anions such as NO_3^-, CO_3^{2-}, SO_4^{2-}, Cl^-, or OH^- to form secondary precipitates of allophane, zeolite A, sodalite, and cancrinite (*5, 8, 11*−*13*). The specific pathway of mineral formation depends on temperature and NaOH concentration. Generally, zeolite A and amorphous feldspathoid form at low temperature (21 C) and low NaOH (0.1 M), but with temperatures above 40 C and high NaOH (>1 *m*) crystalline feldspathoid minerals, sodalite, and cancrinite form (*8, 14*). However, recent geochemical transport modeling predicted that formation of cancrinite can also occur in a flowing system at both ambient and high temperatures (*15*). The caustic solution also creates preferential flow paths due to the dissolution of silicates and increases the proportion of immobile phases (*12*). Continuous addition of dissolved Al in waste solution as well as additional Al supply from dissolution of aluminosilicates encourages the growth of secondary precipitates where contaminants can be retarded by either coprecipitation or sorption (*16, 17*). Definition of sorption here includes all adsorption, absorption, surface precipitation, and coprecipitation processes resulting in removal of sorbate from solution to the sorbent.

Strontium and Cs have been observed to interact with secondary precipitates and not only sorb to or incorporate into precipitates but also direct what type of precipitates form. Deng et al. (*11*) found that the presence of low concentrations of Sr and Cs increased the formation of cancrinite. Strontium and Cs have been found to be incorporated into the cancrinite structure and to sorb to the surface of the secondary precipitates (*7, 11, 13, 18, 19*). Chorover et al. (*20*) found that when a simulated tank waste leachate (STWL) was reacted with Hanford sediments, Sr had a fast initial uptake, and on average 80−90% of Sr was removed from solution regardless of initial Sr concentration, compared to a total uptake of Cs ranging from 10−40% of initial Cs concentrations (*20*).

While Sr and Cs sorption has been extensively studied in batch systems and water saturated columns, little is known about the combined effects of mineral dissolution and precipitation under unsaturated flow on transport of Sr and Cs. The objective of this study was thus to investigate the effects of the formation of secondary precipitates on retardation of Sr and Cs mobility using a pure quartz sand under variably saturated conditions. We used pure quartz sand instead of natural Hanford sediments to isolate the effects of newly formed mineral precipitates on Sr and Cs transport.

Experimental Section

Quartz Sand. Quartz sand (fractionated to 200−300 μm in diameter; Aldrich) was used for batch and column experiments. Before use, the quartz sand was soaked for two days in a 2% nitric acid solution to remove impurities, rinsed with deionized water, and oven-dried at 105 C for 24 h.

Simulated Tank Waste Leachate (STWL). A simulated tank waste leachate was prepared as a surrogate for the mixed radioactive wastes that have leaked into the vadose zone from the Hanford tanks. Reagent-grade chemicals were used to prepare STWL consisting of 2 M Na^+, 1 M OH^-, 1.053 M NO_3^-, 0.053 M Al^{3+}, 10^{-5} M Sr^{2+}, and 10^{-5} M Cs^+. The

* Corresponding author phone: (509)376-4627; fax: (509)376-1638; e-mail: wooyong.um@pnl.gov.
† Pacific Northwest National Laboratory.
‡ Washington State University.

10.1021/es903223x
Published on Web 10/01/2010

TABLE 1. Summary of Batch Adsorption Experiments in STWL with Sr and Cs at Initial Concentrations of 10^{-5} M

conditions			equilibrium concentrations		
atm[a]	quartz	reaction time (days)	Sr (C/C_o)	Sr K_d (mL g^{-1})	Cs (C/C_o)
no	yes	2	0.72	1.29	1.04
no	yes	2	0.71	1.32	1.05
yes[b]	yes	2	0.73	1.23	1.02
yes[b]	yes	2	0.73	1.24	1.01
no	yes	7	0.67	1.62	1.03
no	yes	7	0.67	1.61	1.06
yes[b]	yes	7	0.73	1.19	1.11
yes[b]	yes	7	0.66	1.66	1.06
no	no	7	1.02	0	0.97
no	no	7	0.99	0	1.01
yes[b]	no	7	1.06	0	1.05
yes[b]	no	7	1.05	0	1.10
yes[c]	no	7	1.00	0	1.04
yes[c]	no	7	1.01	0	1.08

[a] Open to atmosphere. [b] Open 3 h per day. [c] Open continuously for 7 days; no quartz indicates control experiments.

measured pH was 14, and the alkalinity by titration showed 45,500 mg L^{-1} as $CaCO_3$. The chemical composition of STWL was similar to those used in related previous experiments (*8, 20*) and represents the lower concentration of the range of chemical compositions found in Hanford tank waste.

Batch Sorption Experiments. Quartz sand (3 g) was mixed with 10 mL of STWL in 15 mL polypropylene centrifuge vials. The vials were either exposed to the atmosphere or closed airtight with screw caps. The "exposed to the atmosphere" vials were opened for three hours each day of the experiment. Four vials were left continuously open to the atmosphere during the experiment as control samples to check for carbonate precipitation. Vials were placed on a moving platform shaker for either 2 or 7 days, after which the supernatant was collected by filtration through a 0.45 μm syringe filter. A summary of the experimental conditions is shown in Table 1. Analysis of Cs and Sr was conducted using an inductively coupled plasma-mass spectrometer (ICP-MS) and an inductively coupled plasma-optical emission spectrometer (ICP-OES), respectively. All reactions were conducted at 21 C in duplicate, including a control sample with no sand added. The final pH did not noticeably change from the pH 13 of the original solution. Additional reactions were also conducted at 21 C for 60 days, and at 75 and 90 C for 30 days, to allow for more pronounced mineral dissolution and secondary precipitation at high temperature by STWL.

Mineral Characterization. The reacted quartz sand was examined for surface morphology and chemical compositions by Scanning Electron Microscopy (SEM) and energy dispersive X-ray spectroscopy (EDS). A X-ray diffractometer (XRD) was used for mineral identification. Synchrotron-based micro-focused XRF and XRD data were also collected at the Advanced Light Source on beamline 10.3.2 [details in the Supporting Information (SI)].

Column Experiments. Acrylic columns (2.54 cm ID and 11.43 cm long) were used with one tensiometer placed at the midpoint of each column. Tensiometers were made of porous ceramic cups (0.67 cm OD and 2.54 cm long) connected to Plexiglas tubes, which were attached to the columns through a 9.53-mm compression fitting. The tensiometers were connected to hanging tube manometers. To minimize the risk of air entry through the bottom assembly of the unsaturated columns, a Permatex RTV silicone gasket maker was used to seal voids. High-purity Teflon tubing (1.59 mm ID) was used for column experiments.

The quartz sand was packed into the columns under saturated conditions with deaired (vacuum) deionized water.

TABLE 2. Conditions and Selected Physical Characteristics of Column Experiments[a]

solution	S_{eff}	Ψ, cm-H_2O	ρ_B, g cm^{-3}	θ, cm^3 cm^{-3}	residence time, d	v, cm d^{-1}
STWL, pH 13	1.0	0	1.69	0.36	0.4	73.2
	0.41	−28	1.65	0.17	0.9	74.4
	0.27	−31	1.62	0.11	2.0	50.6
0.1 M $NaNO_3$, pH 7	1.0	0	1.67	0.37	0.4	94.1
	0.36	−29	1.56	0.16	0.8	96.4
	0.20	−33	1.74	0.074	2.2	69.6

[a] Abbreviations: S_{eff} = effective liquid saturation; Ψ = hydraulic head; ρ_B = bulk density; θ = volumetric liquid content; v = pore water velocity; temperature for column experiments was 21 C.

The columns were intermittently vibrated during packing to ensure uniform packing and minimize air-entrapment. A syringe pump was used for a constant flow rate with adjusting the rate until a steady-state flow was achieved. Input solution was dripped onto the top surface of the unsaturated columns covered with a 30-mbar bubbling pressure nylon mesh filter (35 μm pore diameter) to distribute the introducing solution evenly over the surface of the packed quartz sand. At the bottom end of the columns, a nylon mesh membrane (5 μm pore diameter, 120-mbar bubbling pressure) was placed in contact with the quartz sand. A hanging water column made of Teflon was used to maintain negative pressure (suction) at the membrane (*21*). Uniform saturation was ensured by simultaneously adjusting the flow rate at the inflow and the suction at the outflow so that the tensiometer readings and the applied suction were at the same water head (within ±2 cm-H_2O). Water retention curves were initially developed for the columns using the hanging water column method (*22*) (Figure SI-1).

Column experiments were conducted with the same solutions as used in the batch experiments at 21 C. Columns were run at steady-state flow rates using three different liquid saturations. We first established steady-state flow at a specified liquid saturation in deionized water and then developed a nonreactive Br tracer (2.5×10^{-4} M KBr) breakthrough curve to determine hydrodynamic characteristics of the column at the different flow rates. For STWL, columns were run at effective liquid saturations of S_{eff} = 0.27, 0.41, and 1.0. Column experiments were also conducted using 0.1 M $NaNO_3$ solutions at saturations of S_{eff} = 0.20, 0.36, and 1.0. The liquid saturation was estimated based on the suction measured with the tensiometer and the water retention characteristic based on the van Genuchten water retention model (see eq 1S in the SI and Figure SI-1).

For each liquid saturation, after the initial Br tracer breakthrough was complete, we introduced either STWL or 0.1 M $NaNO_3$ solution containing Sr and Cs, while the flow rates and liquid saturations were kept constant as verified by the tensiometer readings. A second Br tracer breakthrough was also determined with 10^{-3} M NaBr spiked in the STWL to verify the flow regime at S_{eff} = 0.41 and 1.0 in STWL. The final liquid contents of the columns were also verified at the end of the experiments by gravimetric measurements. Table 2 shows a summary of experimental scenarios and selected parameters for the column experiments.

Column effluent was collected with a fraction collector and filtered using 0.45-μm syringe filters. Bromide in the effluent solution was quantified with an ion chromatograph (IC) or ICP-MS. Concentrations of cations were analyzed using ICP-MS for Cs and ICP-OES for Sr, Na, Al, and Si.

Modeling. The dimensionless convection-dispersion equation (CDE) was used to analyze the column data, mainly to determine retardation of Sr and Cs with respect to the conservative tracer Br. We considered both equilibrium and

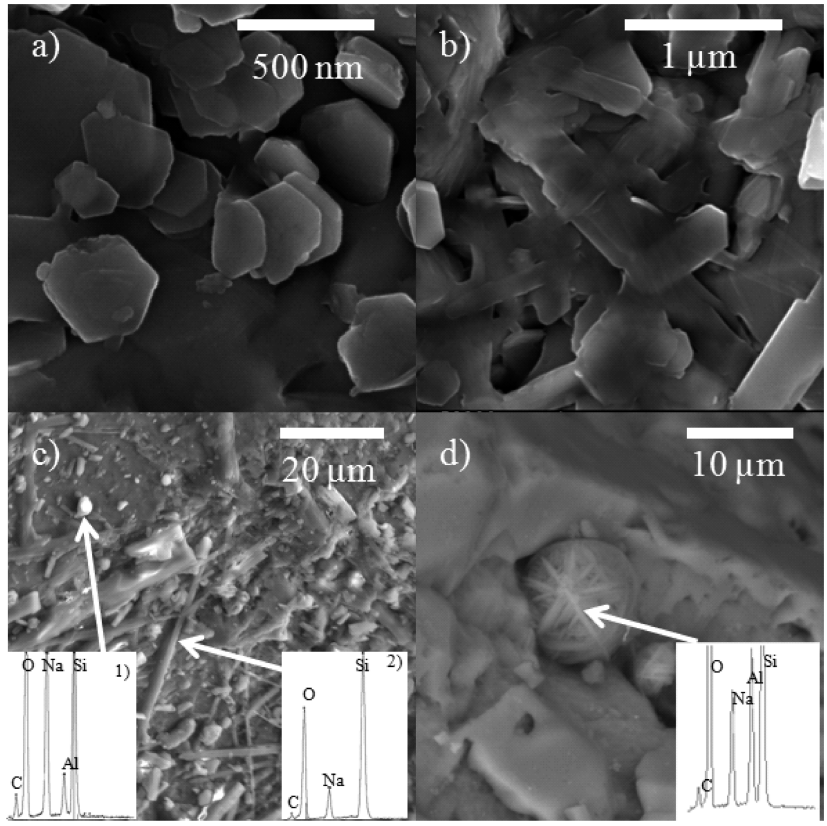

FIGURE 1. SEM images of secondary precipitates formed on quartz sand reacted with STWL (a) initial stage of hexagonally shaped euhedral minerals at 21 C for 30 days; (b) platy minerals at 21 C for 30 days; (c); small cubical and lenticular minerals with EDS spectra of cubical minerals (left) and lenticular minerals (right) at 21 C for 60 days; (d) string ball-shaped cancrinite with EDS at 75 C for 30 days. The carbon peaks in EDS are from the coating of the samples for SEM.

nonequilibrium sorption in modeling. The general nonequilibrium CDE is described in the SI.

We first determined the retardation factor (*R)* for all breakthrough curves by moment analysis (*23*). The dispersion coefficient (*D)* was then estimated from the bromide breakthrough data using CXTFIT (*24*). Transport of reactive solutes (Sr, Cs, and Al) was also modeled using the nonequilibrium model with the fixed *R* value previously estimated from the moment analysis and the *D* value from Br tracer analysis, while optimizing the fraction of nonequilibrium sorption sites (β) and the mass transfer coefficient (ω) between equilibrium and nonequilibrium sites. When β values of 0.98−1.0 were obtained, we used the equilibrium CDE instead of nonequilibrium model.

To support evidence of mineral dissolution and formation of secondary precipitates under the experimental conditions in the columns, we used the geochemical model (Geochemists Workbench 7.1) with thermodynamic data for cancrinite [see details in the SI].

Results and Discussion

Batch Sorption Experiments. When quartz sand was reacted with STWL at atmospheric CO_2(g), the removal of Sr (10^{-5} M) from solution was nearly 30%, consistent with the relative concentration of remaining Sr, $C/C_o = 0.73$ and 0.70 after two and seven days reaction, respectively (Table 1). For treatments closed to atmospheric CO_2(g) during the experiment, a similar amount of Sr (28−33%) was removed from the solution. As there was no measurable Sr removal for the control samples in both open and closed conditions ($C/C_o = 1.0$ in Table 1), we conclude that no precipitation of $SrCO_3$ occurred at 10^{-5} M Sr in STWL. At the Sr concentration of 10^{-5} M, the STWL was undersaturated with respect to $SrCO_{3(s)}$ (saturation index of $10^{-0.17}$), as was also observed by others under similar conditions (*20*). As Sr is excluded from adsorption sites of quartz surface because of the competition by Na in high ionic strength solution (*15*), the removal of Sr (10^{-5} M) in STWL is attributed to Sr incorporation into or sorption onto newly formed secondary precipitates.

An early stage of formation for secondary precipitates can be seen in SEM images for the reacted quartz in batch reactions at 21 C (Figure 1a−c). The images show hexagonally shaped euhedral minerals (Figure 1a), platy structures (Figure 1b), and cubical secondary precipitates (Figure 1c) formed on the quartz surface. The cubical precipitates in Figure 1c contain Na, Al, Si, and O (EDS-left), consistent with chemical composition necessary for crystalline cancrinite formed at 75 C (Figure 1d). String-ball shaped secondary precipitates, typical in morphology of cancrinite (Figure 1d), were found on quartz surface at 75 C. These high temperature secondary precipitates had the same elemental composition as the low temperature secondary precipitates (Na, Al, Si, and O), suggesting that the low temperature precipitate was a precursor of crystalline cancrinite. The geochemical modeling predicts that cancrinite can be formed in this system at temperatures as low as 20 C (Figure SI-2), but we have no direct evidence for crystalline cancrinite on the quartz sand at our experimental temperature of 21 C. Though the Si:Al mole ratio should be 1:1 for cancrinite (*8*), the observed high Si peak in the EDS (Figure 1c) was likely because of initial precipitation stage with relatively low Al concentration and the background quartz contributing to spectral intensity for Si. The needle-shaped particles containing no Al (EDS-right in Figure 1c) may indicate sodium silicate. Mineral identification of these secondary precipitates using XRD was not successful, because of the low abundance of secondary precipitates formed at 21 C. However, supplementary batch

experiments conducted at 90 C confirmed cancrinite formation on quartz surface by XRD analysis (Figure SI-3).

Microfocused XRF of the 75 C sample showed that Sr was spatially correlated with the location of the secondary precipitates (Figure SI-4). As there was no Sr sorption to quartz in STWL and the sample used for microfocused XRF was rinsed with DI water to remove readily dissolvable amorphous phases, leaving only the crystalline cancrinite as seen on the SEM images, Sr was associated with the cancrinite structures. Microfocused XRD on the hot spots of highly concentrated Sr location (green in Figure SI-4a and 4b) also confirmed the presence of cancrinite. Based on this and previous findings from the literature (*19*), we conclude that Sr was being either incorporated into and/or sorbed to the secondary mineral precipitates formed on quartz surface after contact with STWL.

However, there was no measurable removal for Cs in solution after 2 and 7 days reaction, regardless of the batch conditions (Table 1). Though there have been batch experiments showing Cs removal by secondary precipitates, sodalite and cancrinite (*13, 20*), our experimental condition is the first study on the quartz sand with STWL under ambient temperature for shorter contact time (<7 days). Even within this short time period, secondary precipitates could be initiated (Figure 1a−c), but these precursor precipitates did not have the characteristic morphology and structure of crystalline cancrinite formed at high temperatures (Figure 1d). Formation of crystalline cancrinite, at ambient temperatures, generally takes more than one year of aging (*8, 25*). Aging time beyond the run time of this experiment would be required to incorporate Cs into the ε-cage structure of cancrinite which is slightly larger than Cs ionic radius (0.17 nm) (*11*).

Adsorption of Cs to quartz sand has been also studied extensively (*26−28*). Flury et al. (*28*) observed linear adsorption isotherms for Cs up to 2.5×10^{-5} M under 1 to 1000 mM NaCl solution, with showing very low removal of Cs at initial concentrations similar to our experiment (Cs = 10^{-5} M). However, we did not observe measurable Cs removal (C/C_o = 1.0) in any of the batch treatments (Table 1), because of two times higher ionic strength in our experiments.

Because Cs adsorption on surface hydroxyl sites is known to be stronger than Sr under the same background conditions (*29, 30*), higher Sr removal (~30%) than Cs (~0%) in STWL is also attributed to higher affinity of Sr incorporation into secondary precipitates than Cs.

Column Experiments. Transport of Sr in the $NaNO_3$ columns under saturated flow was similar to the transport of the nonreactive Br tracer (Sr R = 1.05; Br R = 1.08) (Figure 2a; Table 3). Strontium has a low sorption affinity to quartz sand, because high Na concentration (0.1 M) competed effectively with Sr for sorption sites on the quartz in $NaNO_3$ column. The same results were obtained for the columns under unsaturated flow: at S_{eff} = 0.36, both Sr and Br behaved as nonreactive tracers (Sr R = 1.19; Br R = 1.14); at S_{eff} = 0.20, Sr and Br moved even faster than expected, but showed similar retardation (Sr R = 0.77; Br R = 0.78) (Table 3). Transport of Cs in the $NaNO_3$ saturated columns showed higher retardation (R = 1.22) compared to that of Sr (R = 1.05), because of higher adsorption affinity of Cs than Sr to silicates (*31*). This retardation of Cs was marginally more pronounced under unsaturated flow (Figure 2b).

In the STWL columns, Sr was retarded the most with an R value of 4.5 for saturated flow, compared to no retardation found in the equivalent 0.1 M $NaNO_3$ columns (Figures 2a and 3a; Table 3), even though STWL has higher Na concentration. The retardation of Sr in the STWL columns corresponds to an effective K_d value of 0.74 mL g^{-1} at S_{eff} = 1.0, 0.88 mL g^{-1} at S_{eff} = 0.41, and 0.74 mL g^{-1} at S_{eff} = 0.27, which is 40% lower than the K_d values determined from the batch tests (K_d = 1.23 and 1.24 mL g^{-1}) (Tables 1 and 3). This discrepancy is not unexpected as it has been found that batch adsorption experiments can over predict adsorption in flow systems because of different solid to solution ratios (*31*).

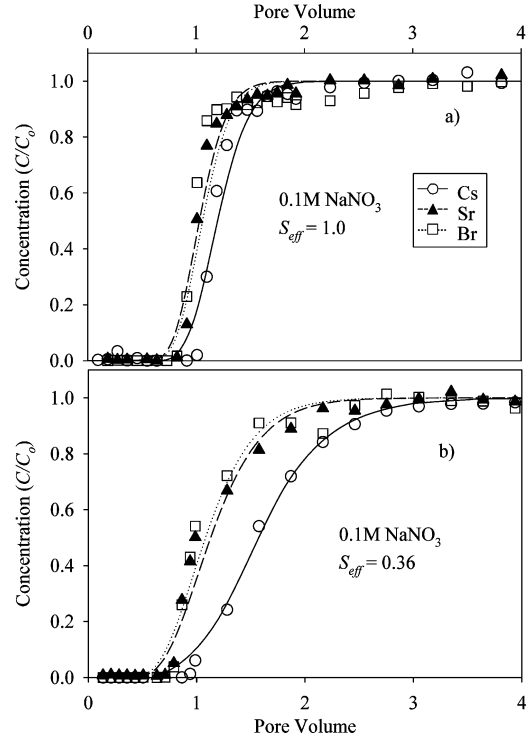

FIGURE 2. Breakthroughs of Cs, Sr, and Br in 0.1 M $NaNO_3$ solution through column packed with quartz sand and model fits for a) S_{eff} = 1.0 and b) S_{eff} = 0.36 at 21 C. Symbols are measured data, and lines are equilibrium model fits.

High concentration of Na effectively limited Sr adsorption to the quartz sand as seen in the 0.1 M $NaNO_3$ columns (Figure 2). In STWL, however, there was pronounced retardation of Sr in the quartz columns (Figure 3), and even more Na was present in STWL. The observed retardation of Sr was attributed to the formation of secondary aluminosilicates on the quartz surface (Figure 1 and Figure SI-4). Strontium can coprecipitate and/or be incorporated into the cage structure of feldspathoid (sodalite/cancrinite) or zeolite formed as secondary precipitates (*7, 19*). At low temperature (21 C) and short reaction time (Table 1), the precipitates included cubic and platy crystals with similar chemical composition to cancrinite, representative of the initial stage of cancrinite precipitates (*5−8, 11*) (Figure 1).

Transport of Cs in the STWL columns showed only little retardation and calculated Cs K_d yielded values of 0.05 mL g^{-1} at S_{eff} 1.0, 0.08 mL g^{-1} at S_{eff} 0.41, and 0.05 mL g^{-1} at S_{eff} 0.27 (Table 3), indicating no significant Cs retardation compared to Sr (Figure 3a) in STWL. Cesium mobility in STWL under unsaturated flow was also similar to Al transport, which suggests no significant removal of Cs related with formation of secondary precipitates (Figure 3b).

Dissolved Al from the STWL, in combination with dissolved Si from the quartz sand, provided the basis for the precipitation of secondary aluminosilicate. However, because of low dissolved Si concentrations (1.47×10^{-3} M for saturated column; 1.7×10^{-3} M and 1.25×10^{-3} M for unsaturated columns), the formation of aluminosilicate precipitates was limited, and complete breakthrough of Al was obtained within 2 and 5 pore volumes in saturated and unsaturated STWL columns, respectively (Figure 3). Assuming a 1:1 mol ratio for Si and Al to form cancrinite as secondary precipitate (*8*), the amount of Al consumed to react with dissolved Si was less than 3% of the initial Al concentration (5.3×10^{-2} M).

TABLE 3. Equilibrium and Nonequilibrium (Two-Site) CDE Model Parameters[a]

solution	S_{eff}	ion	v (cm d^{-1})	R	P	β	ω	r^2	K_d (mL g^{-1})
STWL	1.0	Br	73.2	0.94	70.4	–	–	0.99	0
STWL	1.0	Al	73.2	0.95	70.4	–	–	0.98	0
STWL	1.0	Cs	73.2	1.21	70.4	–	–	0.98	0.05
STWL	1.0	Sr	73.2	4.47	70.4	–	–	0.99	0.74
STWL	0.41	Br	74.4	1.01	46.0	–	–	0.99	0
STWL	0.41	Al	74.4	1.62	46.0	0.43	0.92	0.99	0
STWL	0.41	Cs	74.4	1.82	46.0	0.43	1.14	0.99	0.08
STWL	0.41	Sr	74.4	8.10	46.0	0.97	0.25	0.99	0.88
STWL	0.27	Br	50.6	0.81	56.5	–	–	0.96	0
STWL	0.27	Al	50.6	1.46	56.5	0.42	2.05	0.99	0
STWL	0.27	Cs	50.6	1.68	56.5	0.44	3.07	0.99	0.05
STWL	0.27	Sr	50.6	13.6	56.5	0.72	0.75	0.97	0.74
0.1 M	1.0	Br	94.1	1.08	54.9	–	–	0.90	0
0.1 M	1.0	Cs	94.1	1.22	54.9	–	–	0.98	0.05
0.1 M	1.0	Sr	94.1	1.05	54.9	–	–	0.98	0.01
0.1 M	0.36	Br	96.4	1.14	18.6	–	–	0.97	0
0.1 M	0.36	Cs	96.4	1.64	18.6	–	–	0.99	0.07
0.1 M	0.36	Sr	96.4	1.19	18.6	–	–	0.99	0.02
0.1 M	0.20	Br	69.6	0.78	14.0	–	–	0.99	0
0.1 M	0.20	Cs	69.6	1.43	14.0	–	–	0.97	0.02
0.1 M	0.20	Sr	69.6	0.77	14.0	–	–	0.98	0

[a] Abbreviations: S_{eff} = effective saturation of sand by solution; v = pore velocity; R = retardation factor (determined by moment analysis); D = hydrodynamic dispersion coefficient (determined from bromide breakthrough); P = Peclet number; β = fraction of equilibrium sorption sites; ω = dimensionless mass transfer coefficient; r^2 = coefficient of determination for curve fit to raw data; K_d = partitioning coefficient.

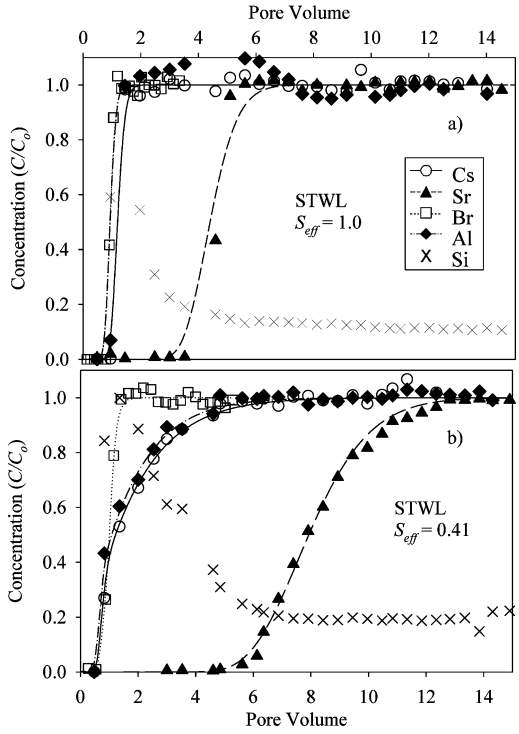

FIGURE 3. Breakthroughs of Cs, Sr, Br, and Al in spiked STWL through column packed with quartz sand and model fits for a) S_{eff} = 1.0 and b) S_{eff} = 0.41 at 21 C. Normalized Si dissolution data based on the highest dissolved Si concentrations (1.47 × 10^{-3} M and 1.25 × 10^{-3} M for S_{eff} = 1.0 and S_{eff} = 0.41, respectively) without model fit are also provided. Symbols are measured data and lines are model fits.

Dissolved Si concentrations from the quartz sand by the STWL are shown in Figure 3. Following an initial increase of dissolved Si concentration, the rapid decrease in Si concentration after 2 pore volumes indicates formation of secondary aluminosilicates (Figure 3). The decrease of Si concentration coincides with an increase of Sr concentration in the column outflow (Figure 3), further supporting that Sr was associated with the neoformed secondary aluminosilicates. We postulate that coprecipitation of Sr onto neoformed secondary precipitates could occur as long as the dissolved Si concentrations were high enough to form cancrinite. As the concentration of dissolved Si from the quartz was reduced, so was the formation of secondary precipitates, consequently Sr was not further removed from solution and could completely break through the columns (Figure 3).

Nonideal Transport. In 0.1 M $NaNO_3$ columns, the breakthrough curves of Br, Cs, and Sr could be modeled well with the equilibrium CDE under both saturated and unsaturated flow (Figure 2 and Table 3). In STWL columns, the breakthrough curves under saturated flow could be also modeled well with the equilibrium CDE. However, under unsaturated flow, there was evidence of nonideal behavior, i.e., deviation from linear sorption and/or equilibrium reactions (Figure 3 and Table 3). This is evident by comparing Sr, Cs, and Al breakthrough curves to the Br breakthrough curve, where Br transported as a conservative tracer and did not show physical or chemical nonequilibrium. Strontium, Cs, and Al all displayed nonideal transport in STWL unsaturated condition. As Br transport could be described well with the equilibrium CDE, we conclude that transport of Sr, Cs, or Al in unsaturated STWL column is either subject to chemical nonequilibrium or nonlinear sorption reactions. The modeling with the nonequilibrium CDE indicates that the data could be well described by this model (Table 3; Figure 3). Nonetheless, we do not have conclusive evidence whether chemical nonequilibrium is the only mechanism causing this nonideal transport, because nonlinear sorption could also cause nonideal behavior, as demonstrated in numerous studies (*31*, *32*).

We postulate that with the rapid initial increase of Si from quartz dissolution, maximum effluent of 35.1 to 48.1 mg L^{-1} Si, there was an initial precipitation of secondary precipitates onto the surface of the quartz along with coprecipitation and sorption of Sr. Strontium appears to be incorporated and/or sorbed to these secondary precipitates, and outflow concentrations of Sr remain low as long as there was an elevated Si concentration in the fluid phase (Figure 3). As soon as Si concentrations decreased, Sr concentrations in the effluents increased, reaching complete breakthrough.

Environmental Implications for Radionuclide Transport. This research was conducted using quartz sand with short contact times and at low temperature; therefore, the results represent the leading edge of the impact from a caustic, Sr and Cs bearing contaminant plume on silicate rich Hanford sediments. Under our experimental conditions, incorporation of Sr into secondary precipitates can be fast and possible even in the early stage of mineral formation, leading to retardation of the movement of Sr. Incorporation of Cs into neoformed feldspathoid (especially cancrinite) is likely to occur slowly depending on the mineral transformation and ripening process, because of the large size of Cs. In a contaminant plume under similar conditions to leaking waste tanks at the Hanford Site, Sr mobility would be preferentially retarded due to coprecipitation and sorption reactions onto the secondary precipitates, but the same coprecipitation reaction would be less measurable for Cs retardation.

Acknowledgments

Funding was provided by the Department of Energy's Environmental Remediation Science Program # DE-FG02-06ER64190. Micro-XRF/XRD works were done by Sunkyung Choi at the University of California, Merced. The Pacific Northwest National Laboratory is operated for the DOE by Battelle Memorial Institute under Contract DE-AC05-76RL01830.

Supporting Information Available

Details of the water retention curve for the quartz column, the convection-dispersion equation, supporting experiments (micro-XRF/XRD) at 75 C and (XRD) at 90 C. This material is available free of charge via the Internet at http://pubs.acs.org.

Literature Cited

(1) Gephart, R. E.; Lundgren, R. E. *Hanford Tank Cleanup: A Guide to Understanding the Technical Issues*, 4th ed.; Columbus, 1998.
(2) Lichtner, P. C.; Felmy, A. R. Estimation of Hanford SX tank waste compositions from historically derived inventories. *Comput. Geosci.* **2003**, *29* (3), 371–383.
(3) Serne, R. J.; Zachara, J. M.; Burke, D. S. *Chemical information on tank supernatants, Cs adsorption from tank liquids onto Hanford sediments, and field observations of Cs migration from past tank leaks*; PNNL-11495; Pacific Northwest National Laboratory: Richland, WA, 1998; p 96.
(4) Zachara, J. M.; Serne, J.; Freshley, M.; Mann, F.; Anderson, F.; Wood, M.; Jones, T.; Myers, D. Geochemical Processes Controlling Migration of Tank Wastes in Hanford's Vadose Zone. *Vadose Zone J.* **2007**, *6* (4), 985–1003.
(5) Bickmore, B. R.; Nagy, K. L.; Young, J. S.; Drexler, J. W. Nitrate-cancrinite precipitation on quartz sand in simulated Hanford tank solutions. *Environ. Sci. Technol.* **2001**, *35* (22), 4481–4486.
(6) Choi, S.; Crosson, G.; Mueller, K. T.; Seraphin, S.; Chorover, J. Clay mineral weathering and contaminant dynamics in a caustic aqueous system - II. Mineral transformation and microscale partitioning. *Geochim. Cosmochim. Acta* **2005**, *69* (18), 4437–4451.
(7) Chorover, J.; Choi, S. K.; Amistadi, M. K.; Karthikeyan, K. G.; Crosson, G.; Mueller, K. T. Linking cesium and strontium uptake to kaolinite weathering in simulated tank waste leachate. *Environ. Sci. Technol.* **2003**, *37* (10), 2200–2208.
(8) Deng, Y. J.; Harsh, J. B.; Flury, M.; Young, J. S.; Boyle, J. S. Mineral formation during simulated leaks of Hanford waste tanks. *Appl. Geochem.* **2006**, *21* (8), 1392–1409.
(9) Mashal, K.; Harsh, J. B.; Flury, M.; Felmy, A. R.; Zhao, H. T. Colloid formation in Hanford sediments reacted with simulated tank waste. *Environ. Sci. Technol.* **2004**, *38* (21), 5750–5756.
(10) Qafoku, N. P.; Ainsworth, C. C.; Szecsody, J. E.; Bish, D. L.; Young, J. S.; McCready, D. E.; Qafoku, O. S. Aluminum effect on dissolution and precipitation under hyperalkaline conditions: II. Solid phase transformations. *J. Environ. Qual.* **2003**, *32* (6), 2364–2372.
(11) Deng, Y. J.; Flury, M.; Harsh, J. B.; Felmy, A. R.; Qafoku, O. Cancrinite and sodalite formation in the presence of cesium, potassium, magnesium, calcium and strontium in Hanford tank waste simulants. *Appl. Geochem.* **2006**, *21* (12), 2049–2063.
(12) Um, W.; Serne, R. J.; Yabusaki, S. B.; Owen, A. T. Enhanced radionuclide immobilization and flow path modifications by dissolution and secondary precipitates. *J. Environ. Qual.* **2005**, *34* (4), 1404–1414.
(13) Mon, J.; Deng, Y. J.; Flury, M.; Harsh, J. B. Cesium incorporation and diffusion in cancrinite, sodalite, zeolite, and allophane. *Microporous Mesoporous Mater.* **2005**, *86* (1−3), 277–286.
(14) Mattigod, S. V.; Hobbs, D. T.; Parker, K. E.; McCready, D. E. *Precipitation of aluminum containing species in tank wastes*; PNNL-13881; Pacific Northwest National Laboratory: Richland, WA, May, 2002; p26.
(15) Zheng, Z.; Zhang, G.; Wan, J. Reactive transport modeling of column experiments on the evolution of saline-alkaline waste solutions. *J. Contam. Hydrol.* **2008**, *97* (1−2), 42–54.
(16) Qafoku, N. P.; Ainsworth, C. C.; Szecsody, J. E.; Qafoku, O. S. Aluminum effect on dissolution and precipitation under hyperalkaline conditions: I. Liquid phase transformations. *J. Environ. Qual.* **2003**, *32* (6), 2354–2363.
(17) Qafoku, N. P.; Ainsworth, C. C.; Szecsody, J. E.; Qafoku, O. S. Transport-controlled kinetics of dissolution and precipitation in the sediments under alkaline and saline conditions. *Geochim. Cosmochim. Acta* **2004**, *68* (14), 2981–2995.
(18) Chen, G.; Flury, M.; Harsh, J. B.; Lichtner, P. C. Colloid-facilitated transport of cesium in variably saturated Hanford sediments. *Environ. Sci. Technol.* **2005**, *39* (10), 3435–3442.
(19) Choi, S.; O'Day, P. A.; Rivera, N. A.; Mueller, K. T.; Vairavamurthy, M. A.; Seraphin, S.; Chorover, J. Strontium speciation during reaction of kaolinite with simulated tank-waste leachate: Bulk and microfocused EXAFS analysis. *Environ. Sci. Technol.* **2006**, *40* (8), 2608–2614.
(20) Chorover, J.; Choi, S.; Rotenberg, P.; Serne, R. J.; Rivera, N.; Strepka, C.; Thompson, A.; Mueller, K. T.; O'Day, P. A. Silicon control of strontium and cesium partitioning in hydroxide-weathered sediments. *Geochim. Cosmochim. Acta* **2008**, *72* (8), 2024–2047.
(21) Cherrey, K. D.; Flury, M.; Harsh, J. B. Nitrate and colloid transport through coarse Hanford sediments under steady state, variably saturated flow. *Water Resour. Res.* **2003**, *39* (6), 1165.
(22) Dane, J. H.; Hopmans, J. W., Water retention and Storage: Laboratory. In *Methods of Soil Analysis, Part 4, Physical Methods*; Dane, J. H., Topp, G. C., Eds.; Soil Science Society of America, Inc.: Madison, WI, 2002; pp 680−683.
(23) Valocchi, A. J. Validity of the local equilibrium assumption for modeling sorbing solute transport through homogeneous soils. *Water Resour. Res.* **1985**, *21* (6), 808–820.
(24) Toride, N.; Leij, F. J.; van Genuchten, M. T. *The CXTFIT code for estimating transport parameters from laboratory or field tracer experiments. Version 2.1*; Report #137; U.S. Salinity Laboratory, U.S. Department of Agriculture: Riverside, CA, 1999; p 117.
(25) Barnes, M. C.; Addai-Mensah, J.; Gerson, A. R. The mechanism of the sodalite-to-cancrinite phase transformation in synthetic spent Bayer liquor. *Microporous Mesoporous Mater.* **1999**, *31* (3), 287–302.
(26) Fukui, M. Evaluation of a combined sorption model for describing cesium transport in a soil. *Health Phys.* **1978**, *35* (4), 555–562.
(27) Saiers, J. E.; Hornberger, G. M. Migration of Cs-137 through quartz sand: Experimental results and modeling approaches. *J. Contam. Hydrol.* **1996**, *22* (3−4), 255–270.
(28) Flury, M.; Czigany, S.; Chen, G.; Harsh, J. B. Cesium migration in saturated silica sand and Hanford sediments as impacted by ionic strength. *J. Contam. Hydrol.* **2004**, *71* (1−4), 111–126.
(29) Turner, N. B.; Ryan, J. N.; Saiers, J. E. Effect of desorption kinetics on colloid-facilitated transport of contaminants: Cesium, strontium, and Illite colloids. *Water Resour. Res.* **2006**, *42* (12), 17.
(30) Oscarson, D. W.; Hume, H. B., Effect of the solid:liquid ratio on the sorption of Sr^{2+} and Cs^{+} on Bentonite. In *Adsorption of Metals by Geomedia*; Jenne, E. A., Ed.; Academic Press: San Diego, CA, 1998; pp 278−288.
(31) Steefel, C. I.; Carroll, S.; Zhao, P. H.; Roberts, S. Cesium migration in Hanford sediment: a multisite cation exchange model based on laboratory transport experiments. *J. Contam. Hydrol.* **2003**, *67* (1−4), 219–246.
(32) Palagyi, S.; Stamberg, K. Modeling of transport of radionuclides in beds of crushed crystalline rocks under equilibrium non-linear sorption isotherm conditions. *Radiochim. Acta* **2010**, *98* (6), 359–365.

ES903223X